HEALTH AND MEDICINE

Reduction of intratumoral brain perfusion by noninvasive transcranial electrical stimulation

G. Sprugnoli[1]*, L. Monti[2]*, L. Lippa[3], F. Neri[1], L. Mencarelli[1], G. Ruffini[4], R. Salvador[4], G. Oliveri[3], B. Batani[3], D. Momi[1], A. Cerase[2], A. Pascual-Leone[5,6], A. Rossi[1,7], S. Rossi[1,7], E. Santarnecchi[1,5†]

Malignant brain neoplasms have a poor prognosis despite aggressive treatments. Animal models and evidence from human bodily tumors reveal that sustained reduction in tumor perfusion via electrical stimulation promotes tumor necrosis, therefore possibly representing a therapeutic option for patients with brain tumors. Here, we demonstrate that transcranial electrical stimulation (tES) allows to safely and noninvasively reduce intratumoral perfusion in humans. Selected patients with glioblastoma or metastasis underwent tES, while perfusion was assessed using magnetic resonance imaging. Multichannel tES was applied according to personalized biophysical modeling, to maximize the induced electrical field over the solid tumor mass. All patients completed the study and tolerated the procedure without adverse effects, with tES selectively reducing the perfusion of the solid tumor. Results potentially open the door to noninvasive therapeutic interventions in brain tumors based on stand-alone tES or its combination with other available therapies.

INTRODUCTION

Glioblastoma (GBM) is the most aggressive and frequent malignant brain tumor. GBM accounts for more than 60% of adult brain neoplasms and affects approximately 10 per 100,000 people worldwide (1). The prevalence of brain metastases (MTX) is estimated to be at least around 9%, with an incidence between 8.3 and 14.3 per 100,000 (2). MTX originate from primary tumors, with the most common ones being the lung (19.9%), melanoma (6.9%), kidney (6.5%), breast (5.1%), and colorectal (1.8%) cancers (2). Despite aggressive treatment combining neurosurgery, radiation therapy, and chemotherapy (2), patients with GBM or MTX have a median postdiagnosis survival window of about 12 months (1).

Electrotherapy (ET) involves the application of a low-intensity direct electric current into the tumor mass by means of two or more platinum electrodes or indirectly, by electrodes placed in the surrounding tissue (3). ET offers some promise in the treatment of bodily tumors and can be combined with chemotherapy (i.e., electrochemotherapy), leveraging its effect by acting on tumor transmembrane permeability and consequently increasing drug concentration in tumor cells (4). Following the first clinical application in patients with lung cancer, ET has been tested on other malignant visceral tumors, including hepatocellular carcinoma, advanced breast cancer, breast hemangioma, and pancreas carcinoma (3). In vivo results have confirmed in vitro findings, showing a reduction of the tumor mass or even prevention of tumor recurrence, with minimal side effects after ET (3). In a pioneering experiment, Jarm and colleagues (5) administered low-intensity DC stimulation (0.6 mA) for 1 hour to subcutaneous fibrosarcoma tumors in mice via two needle electrodes located 5 mm from the tumor's margins. Tumor perfusion (assessed by tissue staining with patent blue violet dye, rubidium ex-

traction technique, and noninvasive near-infrared spectroscopy) was reduced by more than 50%, starting after 15 min of DC stimulation and lasting for almost 24 hours. Moreover, reduction of perfusion was followed by a decrease in tumor size 1 day after the intervention. The decrease in blood flow caused a decrease in tumoral partial oxygen pressure (pO_2), supposedly promoting tumor necrosis (6). Several, not mutually exclusive, mechanisms for ET effects on tumors have been proposed: (i) pH alterations near the electrodes due to electrolysis reaction, (ii) apoptosis, (iii) microembolism, (iv) immunomodulation, (v) toxic derivate of electrochemical reactions, and (vi) vasoconstriction (3, 6).

Noninvasive application of ET to brain tumors requires technological developments. In the current study, we investigated the possibility of affecting brain tumor perfusion via noninvasive electrical DC brain stimulation. To assess brain stimulation–induced cerebral blood flow (CBF) changes, we combined magnetic resonance imaging (MRI) and noninvasive brain stimulation in patients with GBM and MTX. In the last two decades, novel forms of noninvasive, transcranial electrical stimulations (tES) have been tested on healthy participants as well as in patients with various neurological and psychiatric diseases, with the aim of modulating or restoring cognitive, motor, and psychological functions (7, 8). In particular, literature on transcranial DC stimulation (tDCS) suggests that low-intensity electrical stimulation (i.e., <2 mA) delivered transcranially affects cortical neurons' membrane excitability, with effects outlasting the stimulation period (7). However, only a few studies have explored the application of tDCS to modulate brain perfusion in humans (9, 10), with no attempts in patients with brain tumors.

Given the ET findings in bodily tumors, we hypothesized that tDCS would similarly decrease brain tumor perfusion. T1-weighted (T1w) and T2-weighted (T2w) MRI sequences were used to manually segment tumors in patients with GBM and MTX, tracing the solid tumor mass, its necrotic core, and the surrounding tissue affected by edema (Figs. 1 and 2). Biophysical modeling applied to individual anatomical models obtained from T1w images (11) was used to compare the electrical field generated by a large set of tDCS electrode montages in each patient (Fig. 2). Specifically, a genetic algorithm accounting for individual anatomical variability and the conductivity of different tumor tissues was used to identify a stimulation solution inducing (i) the highest electric field over the solid tumor while (ii) minimally affecting the rest of the

[1]Brain Investigation and Neuromodulation Laboratory, Department of Medicine, Surgery and Neuroscience, Unit of Neurology and Clinical Neurophysiology, Siena Medical School, Siena, Italy. [2]Unit of Neuroimaging and Neurointervention, "Santa Maria alle Scotte" Medical Center, Siena, Italy. [3]Unit of Neurosurgery, "Santa Maria alle Scotte" Medical Center, Siena, Italy. [4]Neuroelectrics, Barcelona, Spain. [5]Berenson-Allen Center for Noninvasive Brain Stimulation, Beth Israel Medical Center, Harvard Medical School, Boston, MA, USA. [6]Institut Guttmann, Universitat Autonoma Barcelona, Barcelona, Spain. [7]Department of Medicine, Surgery and Neuroscience, Human Physiology Section, Siena Medical School, Siena, Italy.
*These authors contributed equally to this work.
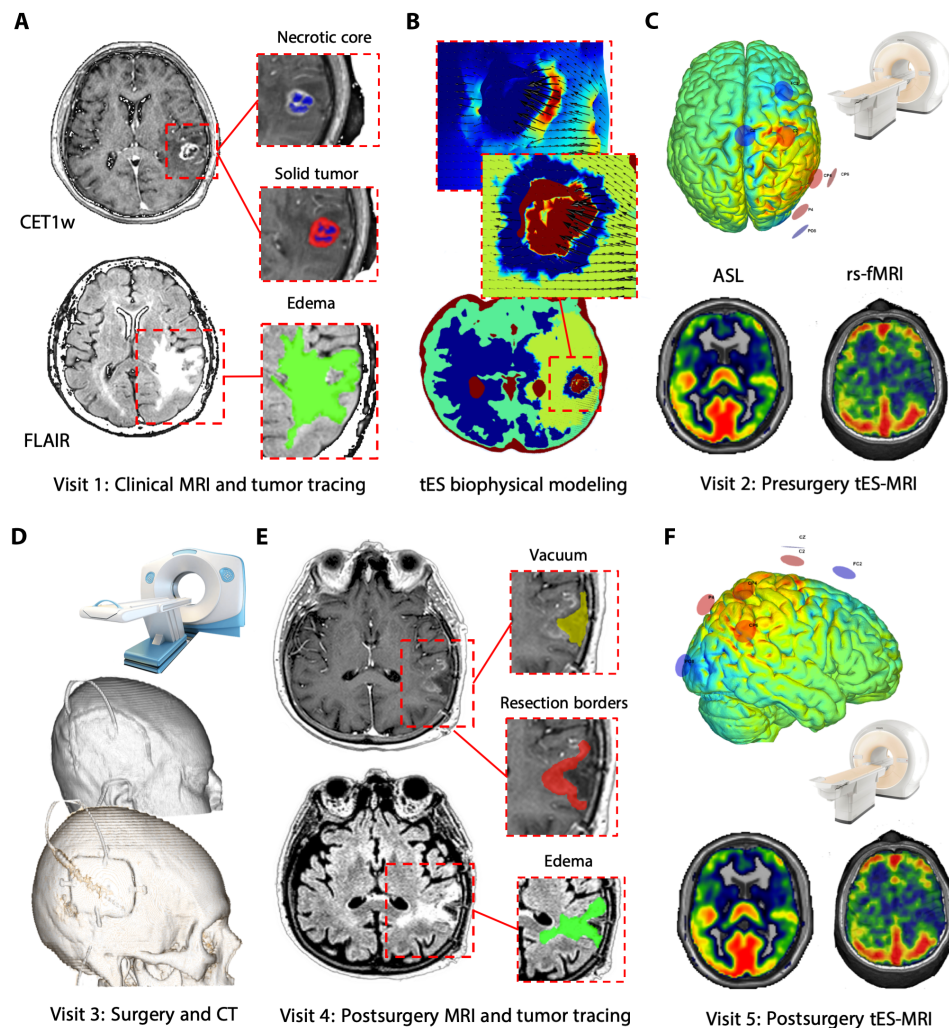†Corresponding author. Email: esantarn@bidmc.harvard.edu

Fig. 1. Experimental design. (**A**) Patients underwent a clinical MRI to define and characterize the brain tumor, including standard and gadolinium-enhanced T1w [CET1w (contrast-enhanced T1w)], T2w, fluid-attenuated inversion recovery (FLAIR), ASL, and resting-state T2-BOLD (blood oxygenation level–dependent) MRI [rs-fMRI (resting-state functional MRI)] images. Regions of interest (ROIs) were defined by parcellating the solid component and the necrotic core of the tumor (MTX in this example) using CE T1w sequences and the edema surrounding the tumor by using FLAIR images. (**B**) Conductivity values were assigned to each ROI as well as to healthy brain tissue according to existing literature (bottom), and then the E-field distribution of current was calculated (top). (**C**) The personalized multielectrode solution maximizing the E-field on the solid-edema interface was selected. The experimental session was planned 3 to 5 days preceding the surgical intervention, and multichannel tES was performed inside the MRI scanner by means of an MRI-compatible brain stimulation device. The stimulation session included the acquisition of (i) T1w, FLAIR, ASL, and rs-fMRI sequences before tES; (ii) rs-fMRI and ASL during tES; and (iii) FLAIR images after tES. (**D**) Roughly 1 week after the presurgery MRI, patients underwent neurosurgery with subsequent histological classification and immediate postsurgery computerized tomography (CT) acquisition. (**E**) Last, approximately 1 month after neurosurgery, selected patients underwent a new MRI acquisition and ROI segmentation to perform a second MRI-tES session (**F**), aimed at evaluating the safety and feasibility of applying tES after neurosurgery. Additional modeling based on CT scan was performed to account for the effects of skull defects created by craniotomy (see also Fig. 3). This was crucial to ensure safety and to study/quantify changes in electric field distribution in the presence of skull defects. Note: All images are presented in neurological convention (right = right).

brain (12). Patients underwent tDCS inside the MRI scanner, while sequences sensitive to CBF, i.e., arterial spin labeling (ASL), and resting-state functional MRI (rs-fMRI) were acquired before and during stimulation. ASL is a noninvasive technique to quantify CBF (i.e., perfusion) without the injection of contrasting agents, leveraging magnetically labeled arterial blood water protons as an endogenous tracer (13). fMRI allows to indirectly quantify neuronal activity by detecting changes in the amount of deoxygenated hemoglobin [expressed by "blood oxygenation level–dependent" (BOLD) signal (14)]. rs-fMRI was added as a control MRI acquisition to verify the selectivity of tDCS effects on perfusion levels. Considering the neurovascular uncoupling

(NVU) caused by gliomas in peritumoral areas [i.e., edema (15)] and the absence of healthy neuronal populations able to respond to electrical stimulation in the tumor region, we hypothesized that tDCS would induce a modulation of perfusion (i.e., CBF) with no changes in BOLD-related indices [i.e., regional homogeneity (ReHo) and amplitude of low-frequency fluctuations (ALFFs)] during stimulation. In selected cases, a tDCS-MRI session after neurosurgery was also carried out, investigating safety and feasibility of tDCS in the presence of skull breaches. In those cases, computed tomography (CT) images were used to carefully model the impact of craniotomy on the electrical field generated in the cortex (Fig. 3).
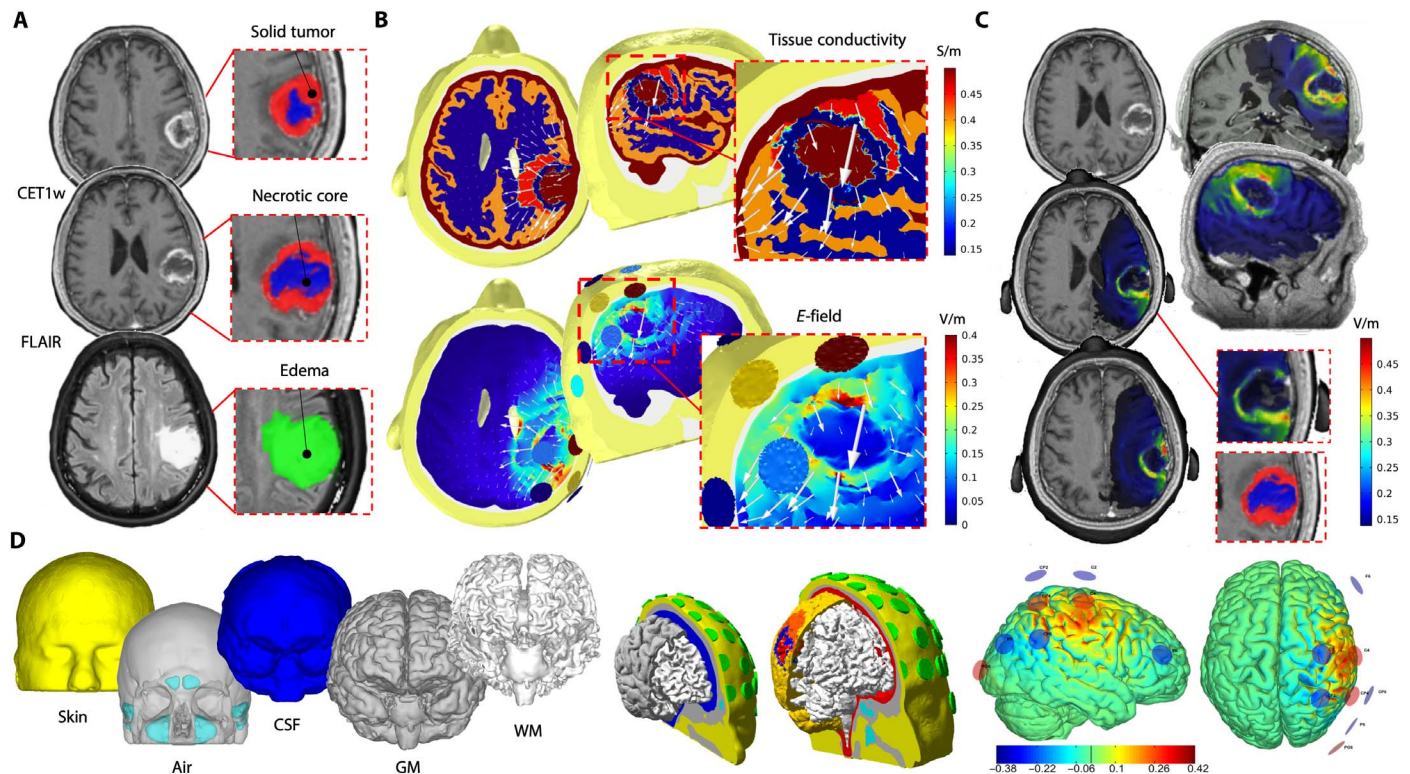
Fig. 2. Tumor tracing, modeling, and optimization. (**A**) MRI images were manually segmented by two independent investigators. Following the Response Assessment in Neuro-Oncology recommendations, the solid part (red) of the tumor (GBM in this example) as well as the necrotic core (blue) were identified on CET1w images. The edema (green) of the tissue surrounding the tumor was segmented using FLAIR images. In the postsurgery phase, T2 Turbo Spin Echo (TSE) scans were used to correctly identify the vacuum created by the surgical intervention. ROIs were manually segmented on the corresponding anatomical scan using MRIcro software and 3D Slicer. ROIs were concentric, with the edema ROI usually including both solid and necrotic parts, while the solid tumor ROI included the necrotic one, such as currently done for planning of radiation therapy. (**B**) Top: Conductivity values were assigned to each ROIs as well as to healthy brain tissue according to existing literature: gray matter (GM) and white matter (WM), cerebrospinal fluid (CSF), skin, and skull. Bottom: A multielectrode solution maximizing stimulation over the edema-solid tumor interface was identified for each patient, with the corresponding E-field distribution calculated on patients' head models. Resulting E-field was overlaid onto individual anatomical T1w scans, showing specificity of the tES solution targeting the solid tumor (**C**). (**D**) In detail, the T1w MRI of the participant was segmented into multiple tissue classes using MARS, SPM-8 segmentation toolbox, and FreeSurfer (left). Models of PITRODE electrodes (cylinders, 1-cm radius) were placed on scalp positions corresponding to the international 10/10 electroencephalography (EEG) system (green circles, center). A genetic algorithm [Stimweaver (12)] was then used to estimate the best multielectrode solution among those possible using 32 positions on the scalp (center), with the final personalized tES montage including up to eight electrodes placed over the hemisphere ipsilateral to the tumor (right). Note: All images are presented in neurological convention (right = right).

RESULTS
Safety
Patients did not experience any clinical or radiological complication during or after tDCS in either pre- or postsurgical tDCS-MRI sessions. During postsurgery tDCS, a notably higher amount of stimulation was estimated to reach the brain/tumor because of current shunting via the skull breaches (Fig. 3). By creating personalized stimulation models accounting for shunting, the maximum value of the electric field magnitude was checked against damage threshold levels based on animal studies, equal to 61 V/m for a current duration of 20 min (7). For all patients, the maximum electric field (E-field) value never exceeded 1 of 13 of this threshold level, and no adverse effects were observed.

Patients were clinically and MRI monitored throughout the entire tDCS-MRI session. First, soon after tDCS, an additional sequence [i.e., fluid-attenuated inversion recovery (FLAIR)] was performed to rule out intracranial complications such as enlargement of the peritumoral edema. Qualitative evaluation of pre- and post-tES FLAIR images did not reveal any significant changes in the edema extension (Fig. 4). Second, patients were monitored for about 1 hour after the tDCS-

MRI before returning to their hospital ward, where standard of care and clinical monitoring were guaranteed. Third, a questionnaire investigating potential tES adverse effects was administered at the end of the tDCS-MRI session (7): Only four patients reported a tingling (consistent with common subjective experience during tES) at the beginning of stimulation that progressively vanished and did not produce any discomfort. Last, routine standard-of-care MRI follow-ups did not show any adverse effects of the intervention. As for patient survival, two patients (numbers 5 and 8) are currently alive, while the remaining cohort died after a mean average of 10 months after the first clinical MRI, in line with the average overall survival (OS) estimated in previous studies (16).

Perfusion and fMRI changes
Cerebral blood flow
A pattern of decreased perfusion induced by tDCS was observed when absolute CBF values were corrected for the CBF of contralateral healthy white matter (WM) (Fig. 5A; see Materials and Methods). In line with the predicted effect, perfusion in the solid tumor displayed a significant
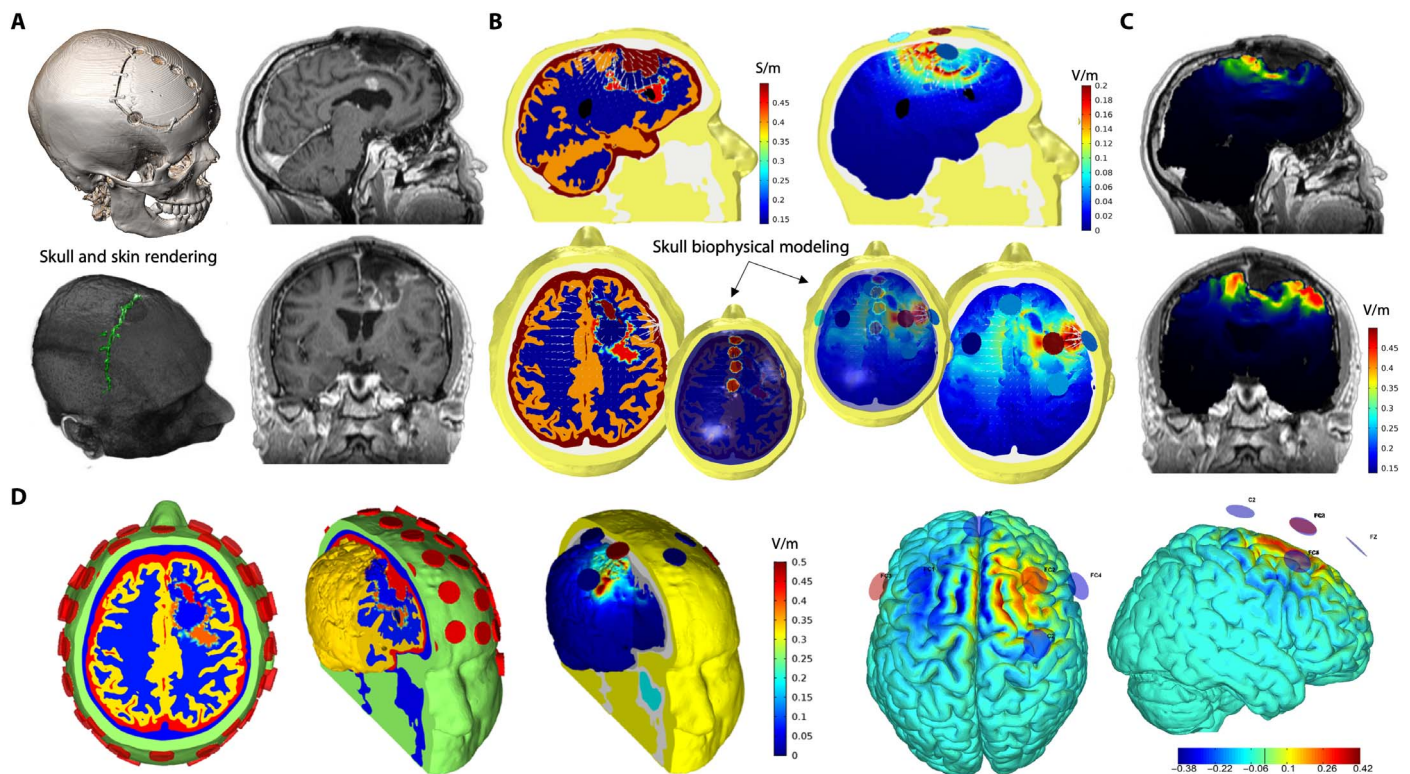
Fig. 3. Postsurgical modeling. (**A**) Structural MRI and CT images were used to model the impact of tES after surgery (shown: complete resection of a GBM). Ad hoc ROIs and three-dimensional (3D) renderings were created for both skull breaches and metallic clips that could respectively influence current shunting and affect electrode positioning. (**B**) New tissue conductivity values were derived by assigning skull defects a conductivity equal to that of the CSF (left), and the amount of current (i.e., E-field) shunting through them was estimated (right). (**C**) A new multielectrode stimulation solution was implemented to maximize stimulation over the resection borders, showing high spatial specificity and control of induced E-field. (**D**) In detail, new geometries of the different head tissues (healthy ones and ROIs) were computed after surgery, leading to a new optimized montage maximizing the current on the surgical borders. Note: All images are presented in neurological convention (right = right).

CBF reduction of −36% (before = 1.784; during = 1.312; $t = 4.653$, $P = 0.001$), ranging from −26% in patients with GBM to −45% in patients with MTX. CBF changes in the necrotic tumor core were not significant (−8.9%, before = 1.272; during = 1.168; $t = 1.124$, $P = 0.294$, ranging from −15% in patients with GBM to −6% in patients with MTX). Similarly, CBF changes were not significant in the area of peritumoral edema (−5%, before = 1.365; during = 1.299; $t = 1.035$, $P = 0.328$, with −8 and −4% in patients with GBM and MTX, respectively).

Control regions
No significant changes in CBF were observed in any of the control regions, with a small increase in CBF both ipsilateral (+5.7%, before = 0.964; during = 1.019; $t = −1.375$, $P = 0.194$) and contralateral (+5.4%, before = 1.064; during = 1.122; $t = −0.692$, $P = 0.502$) to the tumor (Fig. 5B).

rs-fMRI changes
No significant changes were observed with fMRI, neither for ReHo (necrotic core, before = 0.797; during = 0.778; $t = 0.663$, $P = 0.526$; solid tumor, before = 0.809; during = 0.784; $t = 1.585$, $P = 0.147$; edema, before = 0.825; during = 0.814; $t = 1.729$, $P = 0.118$) nor for fractional ALFF (fALFF) (necrotic core, before = 0.258; during = 0.274; $t = −1.642$, $P = 0.139$; solid tumor, before = 0.260; during = 0.270; $t = −1.451$, $P = 0.213$; edema, before = 0.268; during = 0.272; $t = −1.141$, $P = 0.283$) (fig. S1), corroborating on the one hand the hypothesized lack of neuronal response to tES due to NVU (e.g., edema regions) and on the other hand the absence of healthy neuronal populations able to respond to tDCS (e.g., solid and necrotic parts).

DISCUSSION
Traditional applications of tES are aimed at modifying cortical excitability in both the healthy and pathological brains (7). Few studies have investigated the possibility of using tES to modify brain perfusion, and none to date has reported the impact of any tES application in patients with brain tumors. Here, we show that multichannel tDCS in patients with malignant primary or metastatic brain tumors is safe and feasible both before and after surgery and also leads to significant tissue-specific reduction of intratumoral perfusion.

Notably, these results are in line with the reported effects of ET on bodily tumors, where a strong reduction in tumor perfusion—followed by a decrease in volume and necrosis—has been shown (3, 5, 6). Given the safety profile of tDCS, the feasibility of its application in both hospital and home settings, its relatively low cost, and the possibility of its combination with other drug-based therapies, the present findings might lead to additional noninvasive therapeutic options for patients with brain tumors.

Patients with GBM and MTX were selected, considering their high prevalence and poor prognosis (1, 2, 17). Gliomas' perfusion is positively related with the World Health Organization grade and negatively
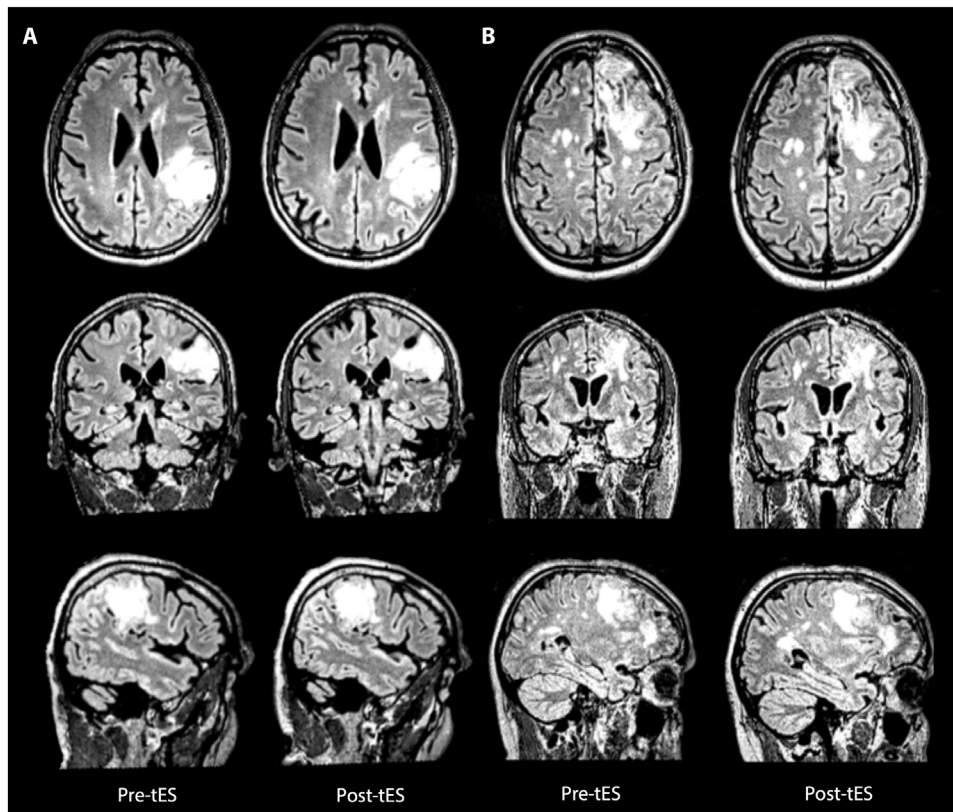
Fig. 4. Safety. FLAIR images acquired before and immediately after tES did not show significant changes in the edema, as shown for two representative patients with GBM at the presurgery (**A**) as well as postsurgery stimulation sessions (**B**). Note: Image constrast was manually adjusted to highlight edema borders. All images are presented in neurological convention (right = right).

correlated with survival (*18*, *19*). In particular, for GBM, neoangiogenesis with increase in vascularization and perfusion are the most distinctive histopathological features, related to extreme invasiveness and aggressive growth (*20*). Moreover, a pattern of hyperperfusion in GBM strongly correlates with the Ki67 index, a well-defined marker of cell proliferation (*21*). Last, CBF and cerebral blood volume represent validated and reliable markers of tumor progression (*22*), and CBF increase detected with ASL is a predictor of a shorter progression-free survival (PFS) and OS (*19*). Therefore, the reported tES-induced reduction in tumor perfusion suggests that repeated applications of tES might have a potential disease-modifying impact. Moreover, the individually tailored brain stimulation solution based on personalized biophysical modeling fits the precision medicine framework, promoting the value of individualized treatments.

From a molecular point of view, vascular endothelial growth factor A (VEGF-A) seems to be the principal mediator of the pathological neoangiogenesis in GBM, correlating also with clinical outcomes (*23*). Considering the importance of inhibiting this specific GBM feature, antibodies targeting the VEGF pathway [i.e., bevacizumab (BEV)] were developed and tested. However, controlled phase 3 trials failed to show a significant effect of BEV on OS in primary GBM (*23*). Other new therapies for GBM include the Optune device (NovoTTF-100A system; Novocure Ltd., Haifa, Israel), recently cleared by the Food and Drug Administration for the treatment of newly diagnosed and recurrent GBM. This noninvasive system delivers low-intensity alternating current transcranially to the tumor [tumor-treating fields (TTFs), 200 kHz; field intensity, >0.7 V/cm at the center of the brain] to inhibit the mitosis of

malignant cells. For the newly diagnosed GBMs, the interim analysis of a randomized phase 3 trial showed that TTF combined with standard chemotherapy (temozolomide) increased the PFS and the OS by about 3 months (*24*). However, for recurrent GBMs, the phase 3 trial did not show any significant improvement of PFS or OS (*25*). Despite the fact that both TTFs and tES are based on electrical stimulation, fundamental technical and conceptual differences exist: (i) TTFs use alternating currents oscillating at extraphysiological frequencies—differently from the DC stimulation used in the present tDCS approach—to impair the proliferation of malignant cells by reducing mitosis; (ii) tES has a good safety profile (*7*), with no adverse effects other than occasional scalp itching and redness, while a variable but considerable percentage of patients receiving TTFs (ranging from 19 to 43%) report dermatological adverse effects such as dermatitis, erosions, ulcers, and infections (*26*); (iii) for TTFs to be effective, patients are required to shave their head and wear the TTF devices more than 18 hours/day during the treatment cycle (4 weeks), whereas tES offers a light and highly portable alternative that usually produces neurophysiological effects (e.g., modulation of corticospinal excitability and cognitive enhancement) even with single, relatively short (i.e., 30 min) sessions. Future studies should compare the two techniques, which could be used as complementary interventions possibly leading to additive effects.

The postulated mechanism for the reduction of tumor perfusion caused by ET on bodily lesions (*5*, *6*) seems compatible with results obtained with tES applications in brain tumors. Occlusion and vasoconstriction of the vessels in proximity to the electrodes have been considered the principal effects of ET, caused by electrolysis occurring around both the
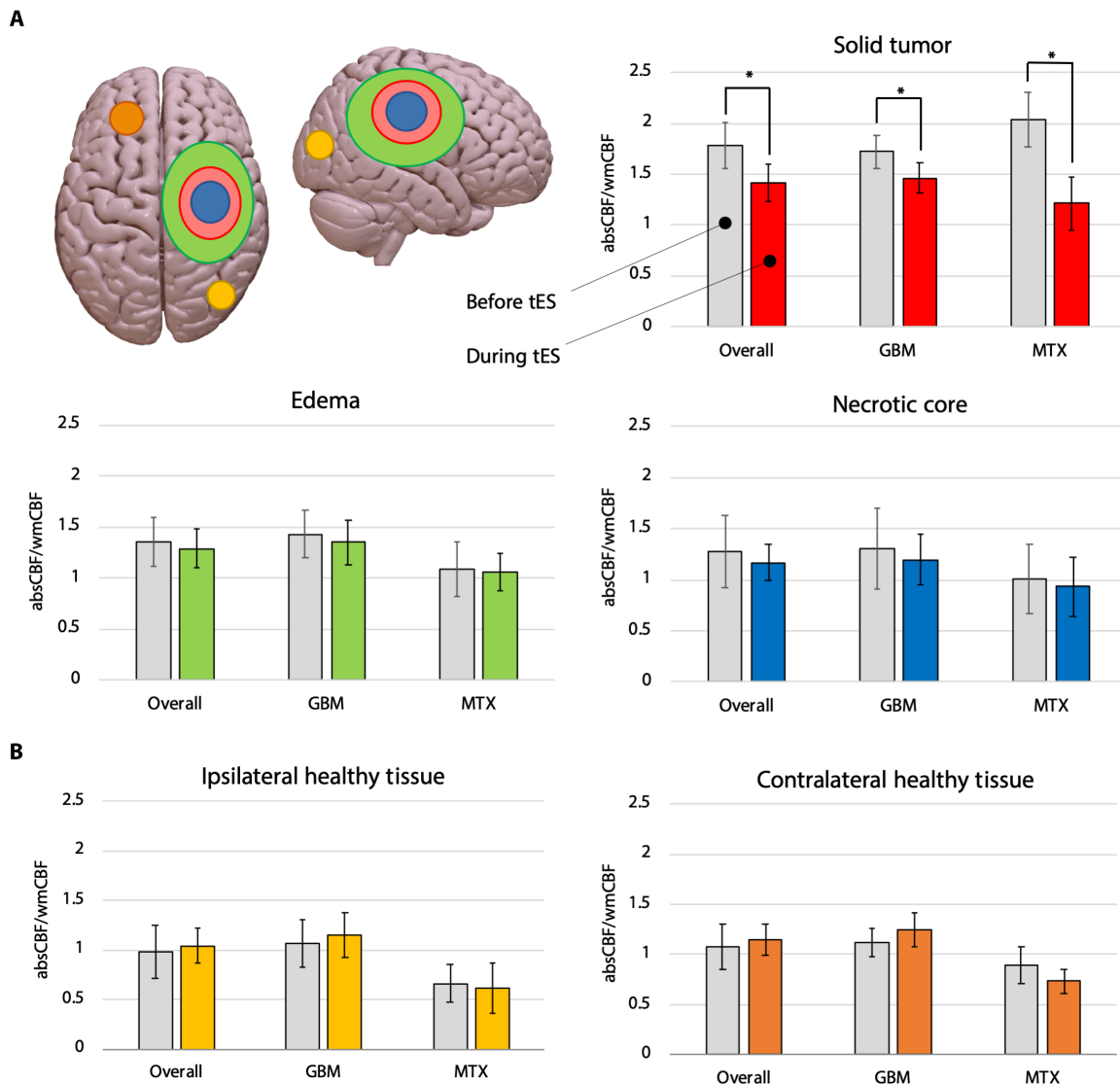
Fig. 5. Perfusion changes. (**A**) Significant reduction in WM-corrected CBF (wmCBF = normalized CBF) was observed in the solid tumor during stimulation for both patients with GBM and MTX (−26 and − 45%, respectively; mean decrease = −36%, *P < 0.001), as compared with no changes in the edema (P < 0.328) and necrotic core (P < 0.294). absCBF, absolute CBF. (**B**) Control ROIs in the contra- and ipsilateral hemispheres to each tumor did not show significant changes in CBF. Note: y axis = normalized CBF calculated as: absolute CBF (ml/100 g per minute)/contralateral WM's CBF (ml/100 g per minute).

cathode and the anode (5, 6). However, how ET selectively affects tumor vessels, leaving the physiological reactivity of vessels of the healthy surrounding tissue unaltered, is not clear. It is possible that the altered micro- and macrostructure characterizing tumor vessels might make them more susceptible to the effects of electric stimulation. These include, for example, lack of smooth muscle cells in the walls, impaired shunts, and higher intercapillary distance in the context of an overall irregular microvascular architecture (3, 27). In addition, the high conductivity of tumors as compared with healthy brain tissues (28), partly due to the abundance of vessels (27), might result in a greater current density inside the tumor. Other mechanisms, such as a possible tES effect on nitric oxide (NO) synthase, cannot be excluded, considering that electrical stimulation has been shown to modify (i.e., increase) NO synthase activity in animal models with consequent increase in tumor blood flow (29). In vitro and in vivo brain tumor models need to be

further explored to disentangle the pathophysiological mechanism underlining tES-induced CBF reduction.

Studies on ET on bodily tumors have shown that the smaller the tumor, the greater the resulting decrease in perfusion. In line with these results, we observed the most important CBF decrease in patients with MTX, representing the smallest lesions in our sample (CBF decrease: −45% in MTX versus −26% in GBM). On the other hand, the different histologic and vascular features of MTX (30) could explain their higher responsiveness to stimulation. However, this hypothesis needs to be tested on a large sample of patients, also considering different types of brain MTX (i.e., colon, breast, and melanoma) and their locations in the cortical mantle, which can influence the amount of current delivered in the tumor.

The present tES protocol only included a single session of 20 min of stimulation at a total intensity across all electrodes of <4 mA, in line with current safety guidelines (7). Stimulation parameters were defined on

the basis of animal studies showing the peak in CBF decrease at around 20′ of continuous ET, while extravasated red blood cells were observed within the lesions—and in many cases, also in the surrounding healthy tissues—after 1 hour of stimulation (6). This phenomenon has been related to leakage of tumor vessels induced by electrolysis and impaired vessel permeability. In addition, the application of single electric pulse to the same tumor model has been shown to lead to a slower recovery to baseline perfusion level after repeated stimulation (31), in line with a similar finding in healthy volunteers receiving multiple tES sessions during ASL imaging (9).

The analysis of variation in perfusion levels in ipsilateral and contralateral regions of interest (ROIs) confirmed the selectivity of tES effects and the accuracy of personalized modeling of induced electric fields. A trend for CBF increase was noticed in the healthy brain tissue in our patients (as opposed to the decrease observed in the tumor's ROIs and compatible with spontaneous brain perfusion fluctuations), suggesting that tES effects were limited to the regions predicted by the biophysical modeling.

BOLD imaging sequences (see fig. S1) were included to verify tES selectivity on perfusion, given the altered neurovascular response (NVU) observed in the tumoral as well as the surrounding healthy brain tissue (15). BOLD-related indices of amplitude and coherence of neurovascular activity (fALFF and ReHo, respectively) did not reveal any significant change during tES in any of the three tumor-related ROIs. fALFF, measuring the amplitude of spontaneous low-frequency fluctuations of BOLD signal, is considered an index of regional spontaneous neuronal activity (SNA), and it had been explored on a variety of psychiatric and neurological conditions (32). ReHo is thought to reflect coherence of local brain activity and has been associated to abnormal activities in many clinical conditions as well (33). Recently, ReHo and ALFF have been explored in relation to the NVU phenomenon in both patients with brain tumors (34, 35) and in a murine brain tumor model (15), with results in line with our findings: The lack of changes in ReHo and fALFF measured in the edema ROI can be related to previously reported peritumoral NVU observed in gliomas, caused by the tumor neoangiogenesis interfering with normal surrounding vasculature (15). On the other hand, we expected no variation in the tumor regions (i.e., solid tumor and necrotic core) considering the lack of healthy neuronal population modifications responding to tES.

The study has some noteworthy limitations. Because of the main goal of establishing safety and feasibility, the sample was small, and we included only two patients with MTX originating both from lung cancer, thus preventing generalization of findings. This also limited the possibility to control for possible markers of prediction to tES response and to investigate potential correlations between changes in perfusion and clinical outcome. In addition, future investigations on preclinical models are needed to address the molecular changes underlining the observed modifications in perfusion levels.

In summary, the present findings support the safety and feasibility of tES in patients with brain tumors, both before and after brain surgery. Electrical stimulation on bodily tumors seems to enhance the effect of chemotherapy treatment (27) by increasing the exposure of malignant cells to chemotherapy, as a consequence of reduced blood flow caused by vessels' vasoconstriction. In addition, a recent study (36) has showed that tES applied on endothelial monolayers [mimicking the healthy human blood-brain barrier (BBB)] can induce a transient, reversible, and polarity-dependent increment in water and solute flux. The possibility to increase transport of molecules across the BBB (e.g., relevant for chemotherapy), along with the reduction of tumor perfusion observed with tES in our patients, opens the possibility of integrating tES with chemotherapy in conditions where surgery represents the primary therapeutic option, as well as when chemotherapy is the only viable solution.

MATERIALS AND METHODS
Sample
During a 9-month period, 50 patients with brain neoplasms, referred to the Neurosurgery and Neuroradiology Units of the "Santa Maria alle Scotte" Medical Center of Siena (Italy), agreed to participate in this study. Only 18 were considered eligible for the study, which had been previously approved by Local Ethical Committee. Participants were screened before the experiment by a multidisciplinary team, including neurologists, radiologists, and neurosurgeons. Inclusion criteria were as follows: (i) age between 18 and 80 years, (ii) valid written informed consent, (iii) strong clinical and radiological suspicion of primary GBM or MTX, and (iv) lesion site presumably reachable by noninvasive stimulation (i.e., cortico-subcortical location). The exclusion criteria were as follows: (i) lesions in deep WM, brain stem, cerebellum, or basal ganglia; (ii) multiple brain lesions; (iii) concomitant radiochemotherapy due to the effect of radiotherapy on tumor perfusion that could alter the assessment of tES effects; (iv) severe dilatation of ventricles; and (v) any health problem or other potential contraindications to undergo the MRI and experimental procedures. Patients were carefully informed about the safety of tES as well as about commonly reported adverse/side effects to ensure informed consent.

After the initial MRI session (Fig. 1A), manual segmentation of the brain tumor was performed in preparation for the tDCS-MRI session (Fig. 1B). Three patients developed health complications before the experimental intervention (thrombocytopenia, status epilepticus, and severe intracranial hypertension) and were excluded. Rapid worsening of clinical conditions led to urgent neurosurgical intervention (2 to 3 days after clinical MRI) in seven patients who were therefore excluded. Stimulation sessions were conducted in eight patients (mean age, 62.5; SD, 13 years; five males and three females; see Table 1): Six were diagnosed with primary GBM and two with MTX from lung cancer. Participants had concomitant neurological conditions: seizures ($n = 2$), focal neurological deficits ($n = 3$), symptoms and signs of endocranial hypertension ($n = 2$); cognitive impairment ($n = 1$). Some patients received corticosteroids, levetiracetam, and heparin ($n = 3$) during the study. Tumors were located in different brain regions: frontal lobe ($n = 4$; two left-sided), parietal lobe ($n = 2$; one left-sided), and temporal lobe ($n = 2$; one left-sided). Histological analyses of patients with MTX classified their lesions as MTX of adenocarcinoma (immunohistochemical patterns: patient 2: TTF1^{+}, CK7^{+}, CKPOOL[±], P15[+], GATA3^{−}; patient 7: CK7^{+}; TTF1^{+}; p63[−]; CDX2^{−}; CK20^{−}). For histological data of patients with GBM, please refer to table S1.

Tumor segmentation
The ROIs for each patient were created on the basis of the presurgical MRI assessment (Fig. 1), independently by two investigators (G.S. and L.Mo.). Following the Response Assessment in Neuro-Oncology recommendations, the solid part of the tumor and the necrotic core were identified on the contrast-enhanced T1w images. One patient with MTX did not show manually identifiable necrosis inside the tumor. The edema in the tissue surrounding the tumor was segmented using FLAIR images. In the postsurgery phase, T2 Turbo Spin Echo (TSE) scans were used to correctly identify the vacuum created by the surgical intervention. ROIs were manually segmented on the corresponding anatomical scan using

Table 1. Patients' data. F, female; L, left; M, male; R, right.

Patient	Age	Gender	Lesion	Location (lobe, side)	Clinical presentation	tES session	Pharmacological treatment
1	46	M	GBM	Frontal, L	Cognitive deficit	Pre- and postsurgery	Corticosteroids, levetiracetam
2	79	F	MTX (lung)	Temporal, R	Seizures	Presurgery	Corticosteroids, levetiracetam
3	67	M	GBM	Frontoparietal, R	Focal neurological deficit	Presurgery	Corticosteroids, levetiracetam
4	77	F	MTX (lung)	Frontal, R	Seizures	Presurgery	Corticosteroids, levetiracetam
5	54	M	GBM	Frontal, R	Endocranial hypertension	Presurgery	Corticosteroids, levetiracetam, heparin
6	45	F	GBM	Temporal, L	Endocranial hypertension	Presurgery	Corticosteroids, levetiracetam, heparin
7	67	M	GBM	Frontal, L	Focal neurological deficit	Pre- and postsurgery	Corticosteroids, levetiracetam, heparin
8	65	M	GBM	Parietal, L	Focal neurological deficit	Postsurgery	Corticosteroids, levetiracetam

MRIcro software (www.mccauslandcenter.sc.edu/crnl/mricro) and 3D Slicer (www.slicer.org/). As presented in Figs. 1 to 3, ROIs were concentric, with the edema ROI usually including both solid and necrotic parts, while the solid tumor ROI included the necrotic core, reflecting what is currently done during radiotherapy planning (37). For the postsurgery stimulations, CT scans of the skull were used to map the skull defects caused by the craniotomy on the T1w images used for biophysical modeling to model the potential shunting of electrical current through the skull defects. T1w images were also used to create a ROI of the metallic clips on the scalp to optimize a tDCS solution with no electrodes close to the postsurgical scar (Fig. 3). Resulting ROIs were compared, and an agreement about the final set of masks to be used for biophysical modeling and neuroradiological analysis was reached by consensus (G.S. and L.Mo.).

Individual head model generation
Individual head models were performed for each participant by using a combination of freely available software tools and custom MATLAB scripts (MathWorks, Natick, MA, USA; www.mathworks.com), following a pipeline derived from (11). T1w MRI images of each participant were segmented into scalp, skull, air, cerebrospinal fluid (CSF), gray matter (GM), and WM masks using a MARS toolbox and an SPM 8 (www.fil.ion.ucl.ac.uk/spm/) segmentation toolbox (Figs. 2 and 3). Models of PITRODE PISTIM 3.14-cm^2 Ag/AgCl electrodes (Neuroelectrics, Barcelona, Spain) were placed in the scalp positions corresponding to the international 10/10 electroencephalography (EEG) system. Finite-element meshes of the head and electrodes were created using Iso2Mesh, a MATLAB toolbox. The meshes were then imported to Comsol (Comsol Inc., Burlington, MA, USA; www.comsol.com), where the E-field calculations were performed. The manually segmented masks of the edema, necrotic core, and solid tumor were used to define the mesh nodes that belong to each of these tissues and used to change the electrical conductivity of the tissues to match that of the lesion. All healthy brain tissue nodes were assigned electrical conductivity values appropriate to DC low-frequency electrical currents: 0.330 S/m (scalp), 0.008 S/m (skull), 10^{-5} S/m (air), 1.790 S/m (CSF), 0.400 S/m (GM), and 0.150 S/m (WM). The conductivity of the necrotic core nodes was set to that of CSF. The conductivities of the solid tumor and edema nodes were defined on the basis of the average WM and GM conductivity values: half of this average conductivity in the solid tumor nodes

(0.138 S/m) and two-thirds higher in the edema nodes (0.458 S/m; see Figs. 2 and 3 for examples), according to prior similar modeling work (38). In three participants, a reevaluation was performed after neurosurgery. Skull defects created by the surgical intervention were manually segmented on T1w images with the guide of the skull CT rendering. Head model regions representing skull defects were assigned a conductivity equal to that of CSF (Fig. 3).

Stimulation montage optimization
tES is usually performed by means of two relatively big (area = 35 cm^2) rectangular scalp electrodes (7). However, these so-called "bifocal" montages do not allow for fine targeting of specific cortical regions because of low spatial resolution of the resulting E-field. In this study, we optimized a solution based on multiple (up to eight) smaller (area = π cm^2) circular electrodes that, when guided by neuroimaging data, can be systematically placed on the scalp to maximize the induced field in the brain over rather small structures, e.g., a brain tumor (12, 39). To achieve such resolution, structural MRI images (T1w) of each patient were preprocessed using the ad hoc pipeline described above. Cortical GM surfaces were obtained and then intersected with the edema as well as solid and necrotic tumor masks, defining a target region aimed at maximizing the normal component of the electric field (E_n) over the intersection of the edema and solid tumor mask (Fig. 2). This target region was then used as input for a genetic algorithm [Stimweaver algorithm (12)] comparing multiple multielectrode montages composed by up to eight stimulating electrodes located on any of the 32 positions of the international 10/10 scalp EEG system. Solutions were found using constrained least-squares minimization to determine the electrode positions and currents that induced a weighted E_n-field that best approximated the weighted target (i.e., the solid tumor). The desired E_n-field was set to 0.25 V/m (the positive value indicates that the target E_n-field is directed into the cortical surface, thus presumed to have an excitatory effect) in the target area. Stimulation was performed using PITRODE PISTIM electrodes (cylindrical 1-cm radius, π cm^2 area, Ag/AgCl/gel electrode; www.neuroelectrics.com), with a maximal current of 2.0 mA at any electrode and a maximal total injected current of 4.0 mA across a maximal number of eight electrodes (Fig. 2). Stimulation was applied for 20 min in a single session inside the MRI scanner. These parameters are within the recommended safety parameters for tES in humans (7).

MRI-tES session

Before starting the MRI-tES session, patients were comfortably seated in a chair, and scalp was gently cleaned with an alcohol solution to improve skin conductivity under the corresponding electrode. An MRI-compatible brain stimulator was used for the tES session (Starstim 8 system, with a multichannel MRI kit, Neuroelectrics, Barcelona, Spain), and participants wore the device throughout the entire MRI session. Conductive rubber electrodes were inserted in circular sponge sockets with a radius of 1 cm, having the same area (3.14 cm^2) as the PITRODE PISTIM used for the head model generation. The sockets were dipped into a saline solution to ensure electric conductivity. Participants were then brought into the MRI scanner, and the electrodes were connected to the MRI-compatible cables. Electrode impedance was checked before launching the first MRI sequence; this also served to ensure that participants were familiarized with the tES-induced scalp sensations (e.g., tingling) before the MRI session. Particular care was taken to minimize head motion via cushions and custom-made padding. Participants were provided with earplugs and were instructed to try to relax and not to move during the MRI acquisition time.

MRI acquisition

MRI scans were performed on a Siemens Avanto Syngo VB17 scanner with a 12-channel head coil (Siemens Medical Solutions, Erlangen, Germany). Pulsed arterial spin-labeled images were acquired using a PICORE Q2T sequence [TR (repetition time) = 3100 ms, TE (echo time) = 22 ms, TI (inversion time) 1 = 800 ms, TI2 = 1600 ms, number of slices = 16, thickness = 6.3 mm, gap = 7.8 mm, imaging matrix = 84 × 84, flip angle = 90°, acquisition duration = 4 min and 45 s]. High-resolution T1w axial images covering the whole brain were acquired using a 3D-MPRAGE sequence (TR = 1880 ms, TE = 3.38 ms, TI = 1100 ms, flip angle = 15°, number of slices = 176, thickness = 1 mm, gap = 0 mm, imaging matrix = 256 × 256). FLAIR images were acquired with a sagittal orientation (TR = 5000 ms, TE = 333 ms, TI = 1800 ms, flip angle = 120°, thickness = 1 mm, number of slices = 176, imaging matrix = 224 × 256). T2 TSE images were acquired with a coronal orientation (TR = 4310 ms, TE = 151 ms, TI = 1800 ms, flip angle = 150°, number of slices = 32, thickness = 4 mm, number of averages = 2, imaging matrix = 444 × 448). Functional images were acquired using a standard echo-planar imaging (EPI) resting state (TR = 2000 ms, TE = 20 ms, flip angle = 70°, number of slices = 37, thickness = 3.59 mm, gap = 4.64 mm, imaging matrix = 448 × 448, acquisition duration = 8 min and 36 s). CT image acquisition was obtained with a BrightSpeed, CT99, GE Hangwei Medical Systems, GE Healthcare scanner. The x-ray source was composed of a single-bend scanning electron beam (120 kV, 320 mA), and volumetric acquisition was based on 96 images (in-plane resolution, 521 × 512; thickness = 1 to 1.3 mm) acquired by using a field of view of 25.0 cm.

ASL preprocessing

Functional imaging data processing and analyses were performed using MATLAB R2014a (MathWorks, Natick, MA, USA; www.mathworks.com), SPM12 (Wellcome Department of Cognitive Neurology, UK; www.fil.ion.ucl.ac.uk/spm), and ASLtbx (https://cfn.upenn.edu/~zewang/ASLtbx.php). The first of 91 ASL volumes was used as the M_0 image, with the remaining 90 volumes used as 45 control-label pairs (labeling first). A six-parameter rigid body motion spatial transformation was used to align the raw EPI time series. Then, the functional images were co-registered to the T1w images. The spurious motion component caused by the systematic label/control alternation was regressed out from the motion parameters before applying the transformation on the images.

Each tag and control pair was subtracted to create 45 perfusion-weighted images. These images were used to create quantified maps of CBF using the software ASLtbx. Specifically, CBF was quantified as ml/100 g per minute (absolute CBF) using the equation recommended by the ASL white paper (13)

$$f = \frac{\Delta M \lambda R_{1a} \exp(\omega R_{1a})}{2M_0 \alpha} \left[1 - \exp(-\tau R_{1a})\right]^{-1}$$

where f is the CBF, ΔM is the difference signal between the control and label acquisitions, R_{1a} is the longitudinal relaxation rate of blood, τ is the labeling time, ω is the postlabeling delay time, α is the labeling efficiency, λ is the blood/tissue water partition coefficient, and M_0 is approximated by the control image intensity. Four-dimensional CBF images were masked to remove out-of-brain voxels and normalized to the Montreal Neurological Institute (MNI) template in SPM12. CBF images were processed using partial volume correction in the native ASL spaces and subsequently normalized to MNI space using a linear affine transformation.

CBF-positive values were extracted from the voxels of the three concentric ROIs (necrotic core, solid tumor, and edema). The edema and solid tumor ROIs were obtained by subtraction (i.e., edema − solid part = real edema defined as "edema" in the manuscript; solid part − necrotic core = real solid, defined as "solid tumor"), while the necrotic ROI was kept the same ("necrotic core"). To verify the selectivity and specificity of the tES effect, we extracted the CBF absolute values from additional ROIs that did not show any sign of tumor invasion at the MRI scans in both the contralateral and ipsilateral hemisphere with respect to the lesion ("control ROIs"). Last, following recent guidelines for CBF analysis, we calculated also the normalized CBF by dividing the CBF absolute values by the healthy contralateral WM's CBF (22).

As a control analysis, quantitative evaluation of CBF were also performed by using the automated Olea Sphere 3.0 postprocessing platform integrated in the MRI scan (Olea Medical SA, La Ciotat, France; www.olea-medical.com). The Bayesian method was applied to motion corrected images to calculate CBF maps. Given that Olea Sphere is designed for clinical reading of ASL images, the software was not suitable for additional custom analyses required by the study design (e.g., correction for CBF values of contralateral WM tissue). CBF values obtained on this platform were compared with those obtained by the ad hoc pipeline developed on MATLAB R2014a, SPM12, and ASLtbx. Raw CBF values were identical for the two pipelines, following the same preprocessing of T1w and ASL data.

fMRI preprocessing

To control for the selectivity and specificity of stimulation on CBF, additional rs-fMRI scans were added to the protocol. ReHo and fALFF indices were extracted with CONN software (www.conn-toolbox.org/). ALFF was considered an index of regional SNA, in contrast to the more classical functional connectivity analysis that provide insight into interregional interactions between areas. fALFF used the ratio of the power spectrum of low frequency (0.01 to 0.08 Hz) to that of the entire frequency range (e.g., 0 to 0.25 Hz for a TR = 2 s) of BOLD signal, allowing to discriminate the signal from liquor cisterns to cortical regions. On the other hand, regional homogeneity (ReHo) was thought to reflect neural synchronization of a given voxel with its neighboring voxels, with higher ReHo value indicating high regional synchronization. In the present analysis, ReHo was calculated according to previous literature calculating the Kendall's coefficient of concordance of the time series of a voxel in relation to those of 26 nearest neighbors.

Statistical analysis

Group-level values introduced to the statistical analyses are reported in Fig. 5. Preprocessed, WM-corrected CBF values acquired before and during tES were compared using paired t test statistics for the entire sample ($n = 10$; 7 before surgery, 3 after surgery), with an α level of 0.05. The analysis was conducted separately for each ROI, i.e., solid tumor (surgical border/residual solid tumor for postsurgery analyses), edema, and necrotic core. Separate paired t test analyses were conducted for ipsilateral/contralateral control regions as well. The same model was used to look at before versus during tES differences in fALFF and ReHo values extracted from solid tumor, edema, and necrotic core. Given the small sample size and independence of each analysis, no correction for multiple comparisons was applied.

Brain surgery and anatomopathological analysis

Approximately 1 week after the first MRI evaluation (Fig. 1), patients underwent brain neurosurgery. Complete resection (defined as the resection of more than 98% of a tumor (40)) was performed on two patients, subtotal resection (defined as the resection between the 50 and 98% of a tumor) on three patients, partial resection (resection of less the 50% of a tumor) on one patient, and biopsy on the remaining two patients. There were no intraoperative complications and postoperative CT scans ruled out postoperative intracranial bleeding, tension pneumoencephalon, ischemia, or brain swelling. See table S1 and the "Sample" section for the immunohistochemical findings.

SUPPLEMENTARY MATERIALS

Supplementary material for this article is available at http://advances.sciencemag.org/cgi/content/full/5/8/eaau9309/DC1
Fig. S1. rs-fMRI changes.
Table S1. Histological data of patients with GBM.

REFERENCES AND NOTES

1. D. A. Reardon, K. L. Ligon, E. A. Chiocca, P. Y. Wen, One size should not fit all: Advancing toward personalized glioblastoma therapy. *Discov. Med.* **19**, 471–477 (2015).
2. M. Valiente, M. S. Ahluwalia, A. Boire, P. K. Brastianos, S. B. Goldberg, E. Q. Lee, E. Le Rhun, M. Preusser, F. Winkler, R. Soffietti, The evolving landscape of brain metastasis. *Trends Cancer* **4**, 176–196 (2018).
3. H. M. C. Ciria, M. M. González, L. O. Zamora, L. E. B. Cabrales, G. V. S. González, L. O. de Oliveira, R. Zanella, A. C. Buzaid, O. Parise, L. M. Brito, C. A. A. Teixeira, M. das Neves Gomes, G. Moreno, V. F. da Veiga, M. Telló, C. Holandino, Antitumor effects of electrochemical treatment. *Chin. J. Cancer Res.* **25**, 223–234 (2013).
4. A. Hills, J. Stebbing, Electrotherapy: Enlightening modern medicine. *Lancet Oncol.* **15**, 1060–1061 (2014).
5. T. Jarm, Y. A. B. D. Wickramasinghe, M. Deakin, M. Čemažar, J. Elder, P. Rolfe, G. Sersa, D. Miklavčič, Blood perfusion of subcutaneous tumours in mice following the application of low-level direct electric current. *Adv. Exp. Med. Biol.* **471**, 497–506 (1999).
6. T. Jarm, M. Cemazar, F. Steinberg, C. Streffer, G. Sersa, D. Miklavcic, Perturbation of blood flow as a mechanism of anti-tumour action of direct current electrotherapy. *Physiol. Meas.* **24**, 75–90 (2003).
7. A. Antal, I. Alekseichuk, M. Bikson, J. Brockmöller, A. R. Brunoni, R. Chen, L. G. Cohen, G. Dowthwaite, J. Ellrich, A. Flöel, F. Fregni, M. S. George, R. Hamilton, J. Haueisen, C. S. Herrmann, F. C. Hummel, J. P. Lefaucheur, D. Liebetanz, C. K. Loo, C. D. McCaig, C. Miniussi, P. C. Miranda, V. Moliadze, M. A. Nitsche, R. Nowak, F. Padberg, A. Pascual-Leone, W. Poppendieck, A. Priori, S. Rossi, P. M. Rossini, J. Rothwell, M. A. Rueger, G. Ruffini, K. Schellhorn, H. R. Siebner, Y. Ugawa, A. Wexler, U. Ziemann, M. Hallett, W. Paulus, Low intensity transcranial electric stimulation: Safety, ethical, legal regulatory and application guidelines. *Clin. Neurophysiol.* **128**, 1774–1809 (2017).
8. E. Santarnecchi, N. R. Polizzotto, M. Godone, F. Giovannini, M. Feurra, L. Matzen, A. Rossi, S. Rossi, Frequency-dependent enhancement of fluid intelligence induced by transcranial oscillatory potentials. *Curr. Biol.* **23**, 1449–1453 (2013).
9. X. Zheng, D. C. Alsop, G. Schlaug, Effects of transcranial direct current stimulation (tDCS) on human regional cerebral blood flow. *Neuroimage* **58**, 26–33 (2011).
10. C. Baeken, J. Remue, M.-A. Vanderhasselt, A. R. Brunoni, S. de Witte, R. Duprat, E. H. W. Koster, R. de Raedt, G.-R. Wu, Increased left prefrontal brain perfusion after MRI compatible tDCS attenuates momentary ruminative self-referential thoughts. *Brain Stimul.* **10**, 1088–1095 (2017).
11. P. C. Miranda, A. Mekonnen, R. Salvador, G. Ruffini, The electric field in the cortex during transcranial current stimulation. *Neuroimage* **70**, 48–58 (2013).
12. G. Ruffini, M. D. Fox, O. Ripolles, P. C. Miranda, A. Pascual-Leone, Optimization of multifocal transcranial current stimulation for weighted cortical pattern targeting from realistic modeling of electric fields. *Neuroimage* **89**, 216–225 (2014).
13. D. C. Alsop, J. A. Detre, X. Golay, M. Günther, J. Hendrikse, L. Hernandez-Garcia, H. Lu, B. J. MacIntosh, L. M. Parkes, M. Smits, M. J. P. van Osch, D. J. J. Wang, E. C. Wong, G. Zaharchuk, Recommended implementation of arterial spin-labeled perfusion MRI for clinical applications: A consensus of the ISMRM perfusion study group and the European consortium for ASL in dementia. *Magn. Reson. Med.* **73**, 102–116 (2015).
14. M. D. Fox, M. A. Halko, M. C. Eldaief, A. Pascual-Leone, Measuring and manipulating brain connectivity with resting state functional connectivity magnetic resonance imaging (fcMRI) and transcranial magnetic stimulation (TMS). *Neuroimage* **62**, 2232–2243 (2012).
15. R. W. Pak, D. H. Hadjiabadi, J. Senarathna, S. Agarwal, N. V. Thakor, J. J. Pillai, A. P. Pathak, Implications of neurovascular uncoupling in functional magnetic resonance imaging (fMRI) of brain tumors. *J. Cereb. Blood Flow Metab.* **37**, 3475–3487 (2017).
16. G. Minniti, G. Lombardi, S. Paolini, Glioblastoma in elderly patients: Current management and future perspectives. *Cancers (Basel)* **11**, 336 (2019).
17. N. D. Arvold, D. D. Shi, A. A. Aizer, A. D. Norden, D. A. Reardon, E. Q. Lee, L. Nayak, I. F. Dunn, A. J. Golby, M. D. Johnson, E. B. Claus, E. A. Chiocca, K. L. Ligon, P. Y. Wen, B. M. Alexander, Salvage re-irradiation for recurrent high-grade glioma and comparison to bevacizumab alone. *J. Neurooncol.* **135**, 581–591 (2017).
18. L. S. Hu, J. M. Eschbacher, A. C. Dueck, J. E. Heiserman, S. Liu, J. P. Karis, K. A. Smith, W. R. Shapiro, D. S. Pinnaduwage, S. W. Coons, P. Nakaji, J. Debbins, B. G. Feuerstein, L. C. Baxter, Correlations between perfusion MR imaging cerebral blood volume, microvessel quantification, and clinical outcome using stereotactic analysis in recurrent high-grade glioma. *AJNR Am. J. Neuroradiol.* **33**, 69–76 (2012).
19. X. J. Qiao, B. M. Ellingson, H. J. Kim, D. J. J. Wang, N. Salamon, M. Linetsky, A. R. Sepahdari, B. Jiang, J. J. Tian, S. R. Esswein, T. F. Cloughesy, A. Lai, L. Nghiemphu, W. B. Pope, Arterial spin-labeling perfusion MRI stratifies progression-free survival and correlates with epidermal growth factor receptor status in glioblastoma. *AJNR Am. J. Neuroradiol.* **36**, 672–677 (2015).
20. N. N. Gatson, E. A. Chiocca, B. Kaur, Anti-angiogenic gene therapy in the treatment of malignant gliomas. *Neurosci. Lett.* **527**, 62–70 (2012).
21. G. A. Alexiou, A. Zikou, S. Tsiouris, A. Goussia, P. Kosta, A. Papadopoulos, S. Voulgaris, A. P. Kyritsis, A. D. Fotopoulos, M. I. Argyropoulou, Correlation of diffusion tensor, dynamic susceptibility contrast MRI and ^{99m}Tc-Tetrofosmin brain SPECT with tumour grade and Ki-67 immunohistochemistry in glioma. *Clin. Neurol. Neurosurg.* **116**, 41–45 (2014).
22. M. Jovanovic, S. Radenkovic, T. Stosic-Opincal, S. Lavrnic, S. Gavrilovic, B. Lazovic-Popovic, I. Soldatovic, R. Maksimovic, Differentiation between progression and pseudoprogresion by arterial spin labeling MRI in patients with glioblastoma multiforme. *J. BUON* **22**, 1061–1067 (2017).
23. J. Jeck, R. Kassubek, J. Coburger, S. Edenhofer, S. S. Schönsteiner, A. C. Ludolph, B. Schmitz, J. Engelke, R. Mayer-Steinacker, J. Lewerenz, L. Bullinger, Bevacizumab in temozolomide refractory high-grade gliomas: Single-centre experience and review of the literature. *Ther. Adv. Neurol. Disord.* **11**, 1756285617753597 (2018).
24. R. Stupp, S. Taillibert, A. A. Kanner, S. Kesari, D. M. Steinberg, S. A. Toms, L. P. Taylor, F. Lieberman, A. Silvani, K. L. Fink, G. H. Barnett, J.-J. Zhu, J. W. Henson, H. H. Engelhard, T. C. Chen, D. D. Tran, J. Sroubek, N. D. Tran, A. F. Hottinger, J. Landolfi, R. Desai, M. Caroli, Y. Kew, J. Honnorat, A. Idbaih, E. D. Kirson, U. Weinberg, Y. Palti, M. E. Hegi, Z. Ram, Maintenance therapy with tumor-treating fields plus temozolomide vs temozolomide alone for Glioblastoma. *JAMA* **314**, 2535–2543 (2015).
25. R. Stupp, E. T. Wong, A. A. Kanner, D. Steinberg, H. Engelhard, V. Heidecke, E. D. Kirson, S. Taillibert, F. Liebermann, V. Dbalý, Z. Ram, J. L. Villano, N. Rainov, U. Weinberg, D. Schiff, L. Kunschner, J. Raizer, J. Honnorat, A. Sloan, M. Malkin, J. C. Landolfi, F. Payer, M. Mehdorn, R. J. Weil, S. C. Pannullo, M. Westphal, M. Smrcka, L. Chin, H. Kostron, S. Hofer, J. Bruce, R. Cosgrove, N. Paleologous, Y. Palti, P. H. Gutin, NovoTTF-100A versus physician's choice chemotherapy in recurrent glioblastoma: A randomised phase III trial of a novel treatment modality. *Eur. J. Cancer* **48**, 2192–2202 (2012).
26. M. M. Mrugala, J. Ruzevick, P. Zlomanczuk, R. V. Lukas, Tumor treating fields in neuro-oncological practice. *Curr. Oncol. Rep.* **19**, 53 (2017).
27. T. Jarm, M. Cemazar, D. Miklavcic, G. Sersa, Antivascular effects of electrochemotherapy: Implications in treatment of bleeding metastases. *Expert Rev. Anticancer Ther.* **10**, 729–746 (2014).
28. B. Song, P. Wen, T. Ahfock, Y. Li, Numeric investigation of brain tumor influence on the current distributions during transcranial direct current stimulation. *IEEE Trans. Biomed. Eng.* **63**, 176–187 (2016).

29. B. F. Jordan, P. Sonveaux, O. Feron, V. Grégoire, N. Beghein, B. Gallez, Nitric oxide–mediated increase in tumor blood flow and oxygenation of tumors implanted in muscles stimulated by electric pulses. *Int. J. Radiat. Oncol. Biol. Phys.* **55**, 1066–1073 (2003).

30. R. R. Langley, I. J. Fidler, The biology of brain metastasis. *Clin. Chem.* **59**, 180–189 (2013).

31. G. Sersa, M. Cemazar, C. S. Parkins, D. J. Chaplin, Tumour blood flow changes induced by application of electric pulses. *Eur. J. Cancer* **35**, 672–677 (1999).

32. S. L. Fryer, B. J. Roach, K. Wiley, R. L. Loewy, J. M. Ford, D. H. Mathalon, Reduced amplitude of low-frequency brain oscillations in the psychosis risk syndrome and early illness schizophrenia. *Neuropsychopharmacology* **41**, 2388–2398 (2016).

33. T. Wu, X. Long, Y. Zang, L. Wang, M. Hallett, K. Li, P. Chan, Regional homogeneity changes in patients with Parkinson's disease. *Hum. Brain Mapp.* **30**, 1502–1510 (2009).

34. S. Agarwal, H. Lu, J. J. Pillai, Value of frequency domain resting-state functional magnetic resonance imaging metrics amplitude of low-frequency fluctuation and fractional amplitude of low-frequency fluctuation in the assessment of brain tumor-induced neurovascular uncoupling. *Brain Connect.* **7**, 382–389 (2017).

35. S. Agarwal, H. I. Sair, J. J. Pillai, The resting-state functional magnetic resonance imaging regional homogeneity metrics–Kendall's coefficient of concordance-regional homogeneity and coherence-regional homogeneity–are valid indicators of tumor-related neurovascular uncoupling. *Brain Connect.* **7**, 228–235 (2017).

36. L. M. Cancel, K. Arias, M. Bikson, J. M. Tarbell, Direct current stimulation of endothelial monolayers induces a transient and reversible increase in transport due to the electroosmotic effect. *Sci. Rep.* **8**, 9265 (2018).

37. S. Fogh, M. Wahl, M. Anwar, D. Haas-Kogan, J. L. Clarke, P. K. Sneed, Standardization and quality assurance of radiation therapy volumes for adults with high-grade gliomas. *Semin. Radiat. Oncol.* **24**, 259–264 (2014).

38. P. C. Miranda, A. Mekonnen, R. Salvador, P. J. Basser, Predicting the electric field distribution in the brain for the treatment of glioblastoma. *Phys. Med. Biol.* **59**, 4137–4147 (2014).

39. G. Ruffini, F. Wendling, R. Sanchez-Todo, E. Santarnecchi, Targeting brain networks with multichannel transcranial current stimulation (tCS). *Curr. Opin. Biomed. Eng.* **8**, 70–77 (2018).

40. N. Ahmadloo, A.-A. Kani, M. Mohammadianpanah, H. Nasrolahi, S. Omidvari, A. Mosalaei, M. Ansari, Treatment outcome and prognostic factors of adult glioblastoma multiforme. *J. Egypt Natl. Canc. Inst.* **25**, 21–30 (2013).

Citation: G. Sprugnoli, L. Monti, L. Lippa, F. Neri, L. Mencarelli, G. Ruffini, R. Salvador, G. Oliveri, B. Batani, D. Momi, A. Cerase, A. Pascual-Leone, A. Rossi, S. Rossi, E. Santarnecchi, Reduction of intratumoral brain perfusion by noninvasive transcranial electrical stimulation. *Sci. Adv.* **5**, eaau9309 (2019).